buildings

MDPI

Article

Flexural Behavior of Corroded RC Beams Strengthened by Textile-Reinforced Concrete

Wei Xie [1], Jie Sheng [1,2,*], Zongjian Yu [2], Yan Li [1] and Guotao Dou [3]

[1] School of Civil Engineering, Xuzhou University of Technology, Xuzhou 221018, China; xiewei@xzit.edu.cn (W.X.); liyan@xzit.edu.cn (Y.L.)
[2] School of Mechanics and Civil Engineering, China University of Mining and Technology, Xuzhou 221116, China; zongjian_yu@cumt.edu.cn
[3] School of Civil Engineering and Architecture, Zhengzhou University of Aeronautics, Zhengzhou 450000, China; zzhydgt@zua.edu.cn
* Correspondence: shengjie@cumt.edu.cn

Abstract: The flexural behavior of corroded reinforced concrete (RC) beams strengthened with textile reinforced concrete (TRC) was analyzed and discussed in this work. Thirteen beams, including one reference beam, three corrosion-only beams, and nine TRC-strengthened corroded beams, were tested under four-point bending. The failure modes, cracks, bearing capacity, load–displacement curves and ductility of the tested beams were analyzed. The results showed that the TRC played a role in increasing the number of cracks and decreasing the width of the cracks in the corroded RC beams. In terms of improving the bearing capacity, TRC can improve the bearing capacity of corroded beams even more than the reference beams, and the strengthening after removing the concrete cover of corroded RC beams is better than direct strengthening. The corroded beams after TRC strengthening exhibited improved ductility. The energy absorption index of the TRC-strengthened corroded RC beams increased with the increase in the number of textile layers.

Keywords: textile-reinforced concrete; corrosion; beam; strengthening; flexural behavior

check for updates

Citation: Xie, W.; Sheng, J.; Yu, Z.; Li, Y.; Dou, G. Flexural Behavior of Corroded RC Beams Strengthened by Textile-Reinforced Concrete. *Buildings* **2023**, *13*, 2902. https://doi.org/10.3390/buildings13122902

Academic Editor: Flavio Stochino

Received: 30 October 2023
Revised: 11 November 2023
Accepted: 14 November 2023
Published: 21 November 2023

Copyright: © 2023 by the authors. Licensee MDPI, Basel, Switzerland. This article is an open access article distributed under the terms and conditions of the Creative Commons Attribution (CC BY) license (https://creativecommons.org/licenses/by/4.0/).

1. Introduction

A reinforced concrete (RC) structure is a commonly used structural form in civil engineering, owing to its reliable performance and cost effectiveness. However, RC structures have durability issues, which cannot be ignored. For example, in a marine environment, the steel bars used in RC structures may corrode. The corrosion products are expansive, causing the concrete cover to crack or even fall off. Moreover, after corrosion, the section bearing capacity and strength of the steel bar decrease. This deteriorates the safety-related properties of the RC structure [1–5], increasing the risk of damage to the concrete structure. To prolong the service life of structures and improve the safety performance of corroded RC beams, strengthening is necessary.

Fiber-reinforced polymers (FRPs) are being increasingly applied to strengthen RC structures. Because an FRP has many merits, such as high specific strength, convenient construction, and corrosion resistance, some researchers have applied it to strengthen corroded RC beams. The results have shown that an FRP reinforcement can significantly enhance the bearing capacity of RC beams [6–8]. However, epoxy resin is mostly used to bond the FRP material on the surface of concrete. This leads to some drawbacks such as lack of high-temperature resistance, poor compatibility with the concrete substrate, and difficulty in pasting on a wet structural surface [9,10].

To overcome the shortcomings of FRP, the textile-reinforced concrete (TRC) strengthening method, using inorganic materials as binders, was proposed. A TRC is composed of textile and fine-grained concrete, which is used to strengthen reinforced concrete (RC) structures owing to its high strength-to-weight ratio, high durability, and ease of installation.

For the research of TRC-strengthened RC structures, Si Larbi [11] et al. and Yin [12] et al. performed a study on the flexural behavior of a TRC-strengthened RC beam. The result showed that TRC can limit the propagation of cracks. The width and spacing of the cracks in TRC-strengthened RC beams can be reduced, and cracks exhibit dense and fine characteristics. D'Ambrisi [13] et al. also conducted a study of the bending performance of a FRCM-strengthened RC beam (The full name of FRCM is fiber-reinforced cementitious matrix, which is another name of TRC). The results showed that the flexural bearing capacity of strengthened beams can be significantly enhanced. Ombres [14] built a model to predict the structural behavior of the FRCM-strengthened RC beam. In terms of the durability of RC beams strengthened with TRC, Yin et al. [15] studied the flexural performance of TRC-strengthened RC beams under the coupling action of load and a chloride wet–dry cycle environment. They found that the stiffness and bearing capacity of TRC-strengthened beams decreased under this environment, however, TRC still maintained good crack control ability. Sheng [16] et al. found that TRC shows a good resistance to freeze–thaw erosion. After 60 freeze–thaw cycles, only a small amount of cement paste peeled off from the surface of the TRC. Mazzuca and Ombres [17,18] studied the residual mechanical properties of FRCM composites and the residual flexural behavior of FRCM-strengthened RC beams after elevated temperature exposure. The results found that the mechanical properties of both FRCM composites and FRCM-strengthened beams remained roughly constant for temperatures ranging from 20 °C to 200 °C, and a significant decrease in the values that were measured at ambient temperature was observed only at 300 °C, which indicated that the FRCM-strengthened method can resist high temperature properly.

In addition to the above research, considering its good mechanical properties and durability, FRCM was also applied to strengthen corrosion-damaged RC beams. Elsanadedy et al. [19], El-Maaddawy et al. [20] and Elghazy [21–23] conducted a bending test on FRCM-strengthened corroded RC beams. The results showed that the failure mode of the strengthened beams depended on the FRCM type. The FRCM can significantly enhance the bearing capacity of corroded RC beams. Compared with the reference RC beam, the ultimate load can be increased by 5%–55%. A similar conclusion was reached in a previous study [24]. Although the preliminary studies have shown that FRCM can improve the flexural behavior of corrosion-damaged RC beams, there are few studies on this aspect, especially considering the wide variety of constituent materials of FRCM, which limits the comprehensive understanding of the flexural behavior of FRCM-strengthened corroded RC beams.

The aim of this paper is to further study and better understand the flexural behavior of a corroded RC beam strengthened with TRC and provide relevant data. In this work, thirteen beams, including one reference beam, three corrosion-only beams, and nine TRC-strengthened corroded beams were designed. The test parameters included the corrosion level, strengthening method (whether repair was performed before strengthening by TRC or not), strengthening scheme (single-sided or three-sided reinforcement), and the number of textile layers added. The failure progress, crack control ability, bearing capacity, load–displacement behavior, and ductility performance of TRC-strengthened corroded RC beams are discussed in this paper. The obtained results can help ensure the safety of structures built in marine environments.

2. Materials and Methods

2.1. Test Specimen and Materials

Thirteen RC beams were designed according to GB 50010-2010 [25] and cast in a laboratory. One of them was not corroded nor strengthened; it was used as the reference beam. Three RC beams were corroded but not strengthened; these were the corrosion-only beams. The other nine beams were corroded first and then strengthened with the TRC. All the RC beams were 2200 mm long, 150 mm wide, and 300 mm high. The size of the RC beams was chosen according to the laboratory conditions. The tensile reinforcement arrangement at the bottom was composed of two ribbed bars, the diameter of which was

14 mm. Two ribbed steel bars were used as reinforcements, and their diameter was 8 mm. To avoid shear failure, stirrups with a diameter of 8 mm were configured. In the shear spans, the space between stirrups was 100 mm. In the pure bending section, the space between the stirrups was 200 mm. Figure 1 shows the geometric dimensions of the tested beams.

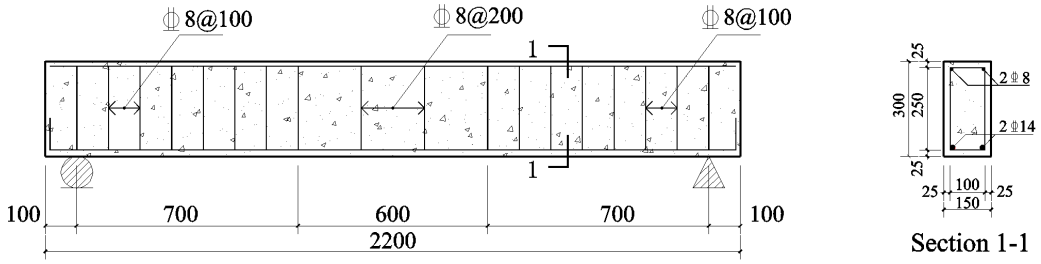

Figure 1. Dimensions and reinforcement of the reference RC beam (unit: mm).

Ready-mixed concrete was used for pouring the RC beams. In accordance with GB/T 50107-2010 [26], three concrete cube specimens with a side length of 150 mm were prepared to measure the concrete strength. The actual measured average compressive strength after the 28-day standard curing period was 38.4 MPa. According to GB/T 228.1-2010 [27], the actual measured yield strength of the tensile reinforcement was 442 MPa, and the actual measured ultimate strength of the tensile reinforcement was 616 MPa. The elongation of the tensile reinforcement was 23.45%.

2.2. Accelerated Corrosion Process

The electrochemical accelerated corrosion technique was used in the manufacturing of the corroded RC beams. This method is efficient and has repeatability in controlling the corrosion degree of steel. The steps in the electrochemical accelerated corrosion are described in the following.

The accelerated corrosion of RC beams is shown in Figure 2. The RC beams were placed into a self-made, leak-proof wooden box after curing for 28 days, and an NaCl solution with a mass fraction of 5% was added into the wooden box. The height of the NaCl solution was controlled to be equal to the thickness of the concrete cover, the purpose of which was to make the steel bar produce an uneven corrosion as far as possible, and to ensure that a sufficient amount of oxygen can participate in the reaction during the corrosion process. To make the chloride ions to fully penetrate the concrete cover, the RC beams were immersed in the solution for 72 h. Current at a density of 300 $\mu A/mm^2$ was then applied to the tensile steel bars. The corrosion level of the steel bar can be expressed using the corrosion rate, which can be obtained using Equation (1). Faraday's law, expressed in Equation (2), was used to obtain the mass loss of the steel bars in theory. The target corrosion levels were 5%, 10%, and 15%, respectively. An insulating tape was wound on the outside of all the stirrups to prevent their corrosion.

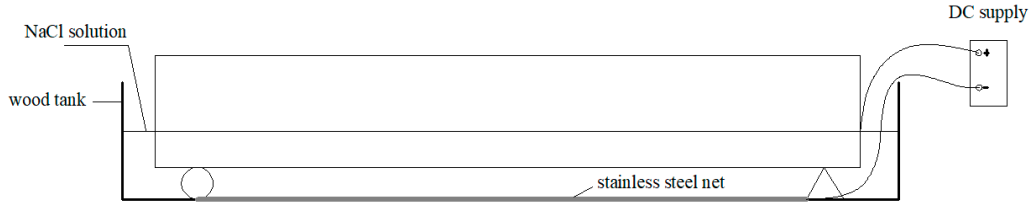

Figure 2. Schematic of accelerated corrosion.

The steps to measure the actual corrosion rate of the steel bars were as follows: (1) cut a 100 mm-long corroded steel bar after completing the bending test; (2) immerse the corroded steel bar into 12% dilute hydrochloric acid until the rust is cleared; (3) use lime water ($Ca(OH)_2$) to neutralize the 12% dilute hydrochloric acid; (4) use distilled water

to wash the corroded steel bar and a dryer to dry them; (5) and weigh the dried corroded steel bars using an electronic scale. The actual corrosion rate can be calculated using Equation (1):

$$\eta = \frac{\Delta m}{m} \tag{1}$$

$$\Delta m = \frac{MI}{Fnt} \tag{2}$$

where η is the corrosion rate; m is the original mass of steel; Δm is the mass loss (in grams); n is the number of electrons transferred during the corrosion reaction (n = 2 for iron); F is Faraday's constant (96,500 C/mol); t is the corrosion duration (in s); I is the applied current (in Ampere); and M is the atomic mass of iron (55.847 g).

2.3. TRC Composite

2.3.1. Textile

Figure 3 shows the textile made of carbon fiber (commercial designation CFN 200/200) that was used in this experiment. The dimensions of the textile were 20 mm × 20 mm. The fiber rovings in the textile were arranged in two orthogonal directions. Table 1 presents the mechanical properties provided by the manufacturer and the test standard is GB/T 1447-2005 [28].

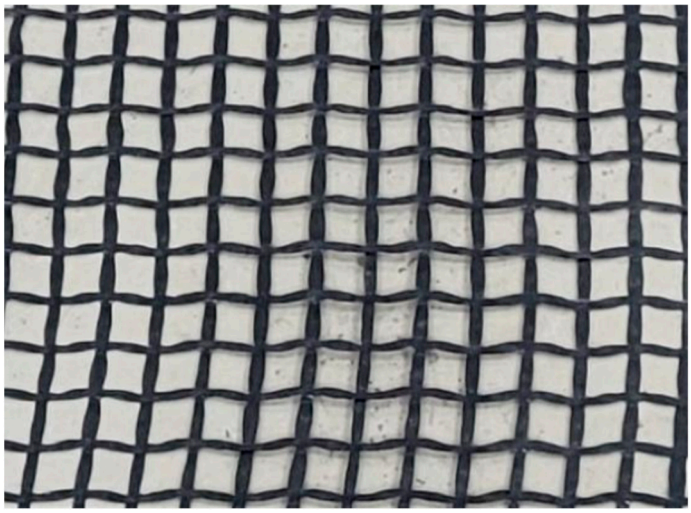

Figure 3. Textile made of carbon fiber that was used in this experiment.

Table 1. Mechanical properties of the carbon fiber rovings in the textile used in this study.

Direction of Fiber	Tensile Strength/MPa	Ultimate Strain/%	Elastic Modulus/GPa
Longitudinal	5110	2.1	246
Transverse	4815	1.9	252

2.3.2. Fine-Grained Concrete

The matrix material of the TRC was fine-grained concrete, with characteristics such as good fluidity and self-compacting and anti-segregation properties. Table 2 shows the mix ratio of the fine-grained concrete. As listed in Table 2, the type of Portland cement used was P·II 52.5R, which is a commercial cement available in China. The particle size range of the fine sand was 0–0.6 mm. The particle size range of the coarse sand was 0.6–1.2 mm. Polycarboxylic acid, which is a high-performance water reducer, was used as the superplasticizer. In accordance with JGJ/T70-2009 [29], three cubic specimens with a side length of 70.7 mm were prepared to measure the compressive strength. The actual

measured average compressive strength after the 28-day standard curing period was 43.2 MPa.

Table 2. Mix ratio of the fine-grained concrete used in this study (kg/m^3).

Cement	Fly Ash	Silica Fume	Water	Fine Sand	Coarse Sand	Super Plasticizer
475	168	35	262	460	920	9.1

2.4. Strengthening Procedure and Configuration

Two different strengthening methods (strengthening methods A and B) were adopted to strengthen the corroded RC beam. In strengthening method A, the corroded beam was directly strengthened using the TRC. In strengthening method B, the concrete cover was removed, and all the corrosion products of the steel bar (Figure 4a) were removed, and the fine-grained concrete was used to repair it to the original section size of the RC beam (Figure 4b), after which the repaired beam was strengthened with TRC. Please note that the strengthening procedure is not standardized.



(**a**) (**b**)

Figure 4. Strengthening method B: (**a**) removing the deteriorated concrete; (**b**) casting fine-grained concrete.

Regarding the strengthening scheme, single-sided and three-sided schemes were considered. The single-sided scheme is bottom-only strengthening of the RC beam (Figure 5a). In the three-sided scheme, both the bottom and side surfaces of the RC beam were strengthened (Figure 5b). The TRC length of both the single-sided and three-sided schemes was 1800 mm. The side height of the three-sided scheme was 75 mm.

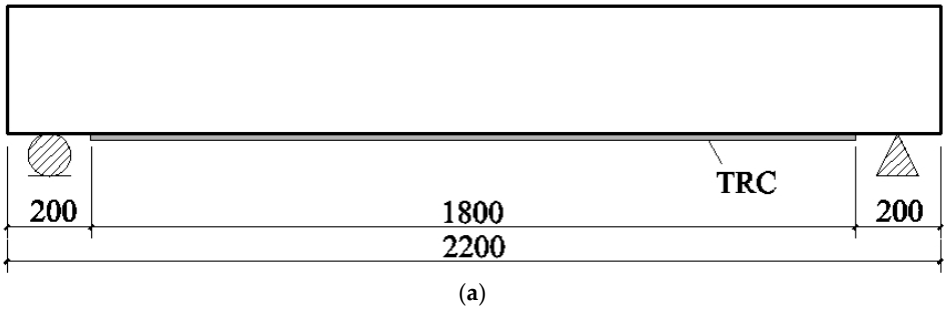

(**a**)

Figure 5. *Cont.*

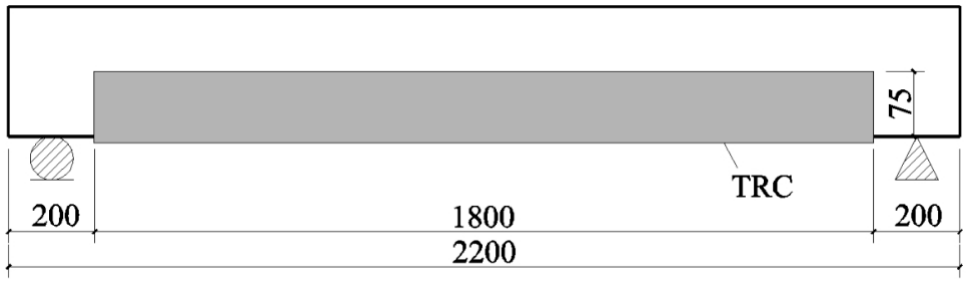

(**b**)

Figure 5. Schematics of the strengthening scheme: (**a**) single-sided scheme; (**b**) three-sided scheme.

Table 3 presents the basic information of each tested beam. The naming method of the tested beam is as follows: M-5/10/15 shows that the corrosion rate of the specimen is 5%, 10% or 15%, S represents the single-sided scheme, and T represents the three-sided scheme. L1, L2, and L3 represent one-layer, two-layer, and three-layer textiles, respectively. A and B represent the strengthening methods A and B, respectively.

Table 3. Basic parameters of the test beams.

Spec.	η/%	Strengthening Scheme	Number of Layers	Strengthening Method
M-0	0	/	/	/
M-5	5	/	/	/
M-10	10	/	/	/
M-15	15	/	/	/
M-5-SL2A	5	single-sided	2	A
M-5-TL2A	5	three-sided	2	A
M-5-TL2B	5	three-sided	2	B
M-10-SL2A	10	single-sided	2	A
M-10-TL2A	10	three-sided	2	A
M-10-TL1B	10	three-sided	1	B
M-10-TL2B	10	three-sided	2	B
M-10-TL3B	10	three-sided	3	B
M-15-TL2B	15	three-sided	2	B

2.5. Loading and Measurement

Figure 6 shows the loading diagram. The four-point bending loading method was adopted. The span of the tested beam was 1800 mm. The length of the shear span was equal to the pure bending section, both of them being 600 mm. The loading device was a hydraulic jack with a maximum loading magnitude of 500 kN. The displacements at the mid-span, support, and loading point were measured using a displacement meter. The 100 mm-long electrical resistance strain gauge was adopted to measure the mid-span concrete strain. A total of six strain gauges of this type were attached to the concrete surface. Taking the top surface of the beam as a reference, the distances of the installed strain gauges from the top to the bottom of the beam were 0, 25, 50, 100, 150, and 225 mm. A 3 mm-long electrical resistance strain gauge was used to measure the strain responses of the tensile steel bars. This type of strain gauge was attached at the middle of the longitudinal steel bar. All the data were recorded using a data acquisition system.

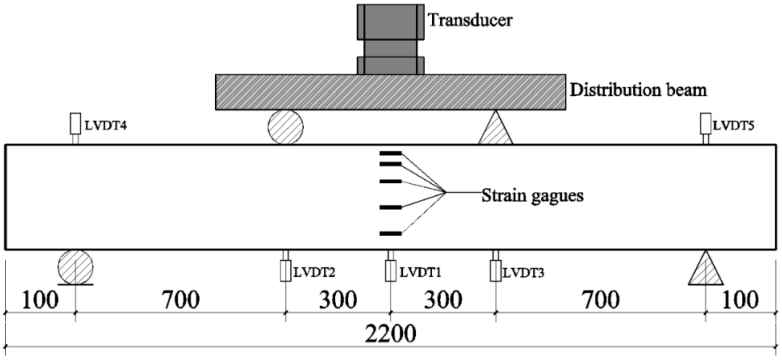

Figure 6. Loading diagram (Unit: mm).

3. Results

3.1. Failure Mode

Figure 7 shows the final damage forms of each tested beam. In the reference beam M-0 and corrosion-only beams M-5, M-10, and M-15, a typical flexural failure mode occurred, that is, the longitudinal steel bar yielded first, and then the compression-zone concrete was crushed. Regarding the failure characteristics of the TRC-strengthened corroded beam, the longitudinal steel bar yielded first, and then the textile layer exhibited a tensile failure, after which the compression-zone concrete was crushed. However, the damage forms of the TRC layers were different. Accordingly, the TRC-strengthened corroded beams exhibited four different failure modes, which can be summarized as follows:

1. Similar to the flexural failure of RC beams, the specimens M-5-TL2B, M-10-TL1B, and M-10-TL2B exhibited this failure mode. In terms of the failure progress, after the steel bar yielded, the sound of some of the fiber bundles being pulled off could be heard with increasing load, indicating that the force acting on the textile was not uniform. With increasing load, the remaining fiber bundles could not withstand the external load and were suddenly pulled off. At this time, due to the redistribution of the internal forces, the compressive stress in the compression-zone concrete suddenly increased, and the concrete was crushed.
2. Partial debonding of the TRC: In this failure mode, the longitudinal steel bar yielded first, and then the TRC layer was partially unbonded; however, the beam could still continue to bear the load at this time due to the sufficient bond length. With increasing load, the textile was completely broken, and the compression-zone concrete was crushed. The beams M-5-SL2A, M-5-TL2A, M-10-SL2A, and M-10-TL2A exhibited this failure mode. This may be because of the poor bonding performance between the TRC and the existing concrete due to corrosion. However, only partial debonding occurred because the TRC bond was long enough.
3. Textile separation from the matrix: In this failure mode, the longitudinal steel bar yielded first, and then the textile separated from the matrix. At this time, the TRC-strengthened corroded beam could not continue to carry the load, and the compression-zone concrete was crushed. Only a part of the fiber bundles was broken when the TRC-strengthened beams was damaged. The M-10-TL3B specimen exhibited this type of failure mode.
4. Fiber slip accompanied by matrix shedding: After the beam entered the yield, the slip between the fiber bundle and the matrix was first generated. With increasing load, the matrix began to fall off. The bearing capacity was finally lost. The beam M-15-TL2B exhibited this failure mode. The reason for this failure mode was the poor adhesion between the fiber and the matrix.

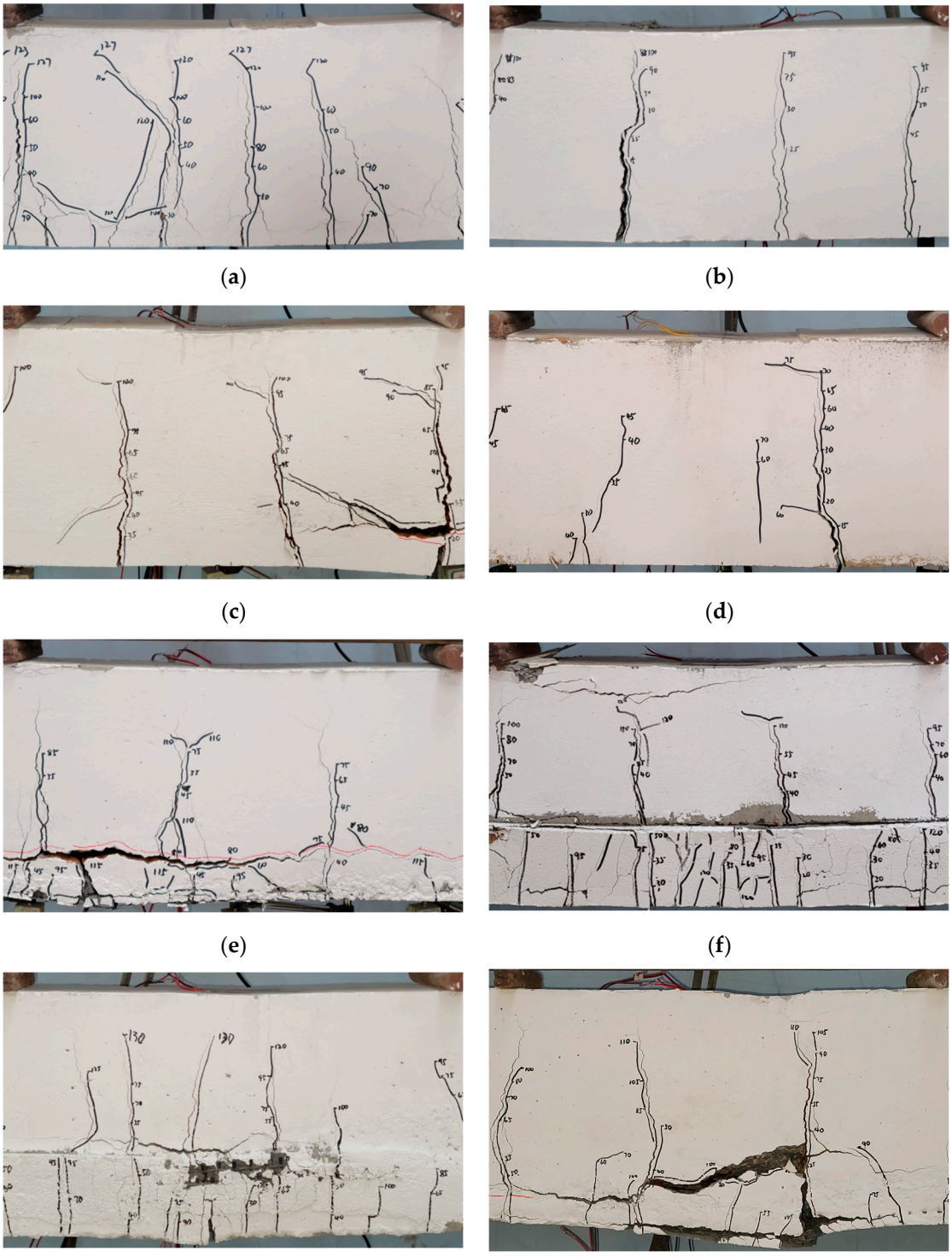

Figure 7. *Cont.*

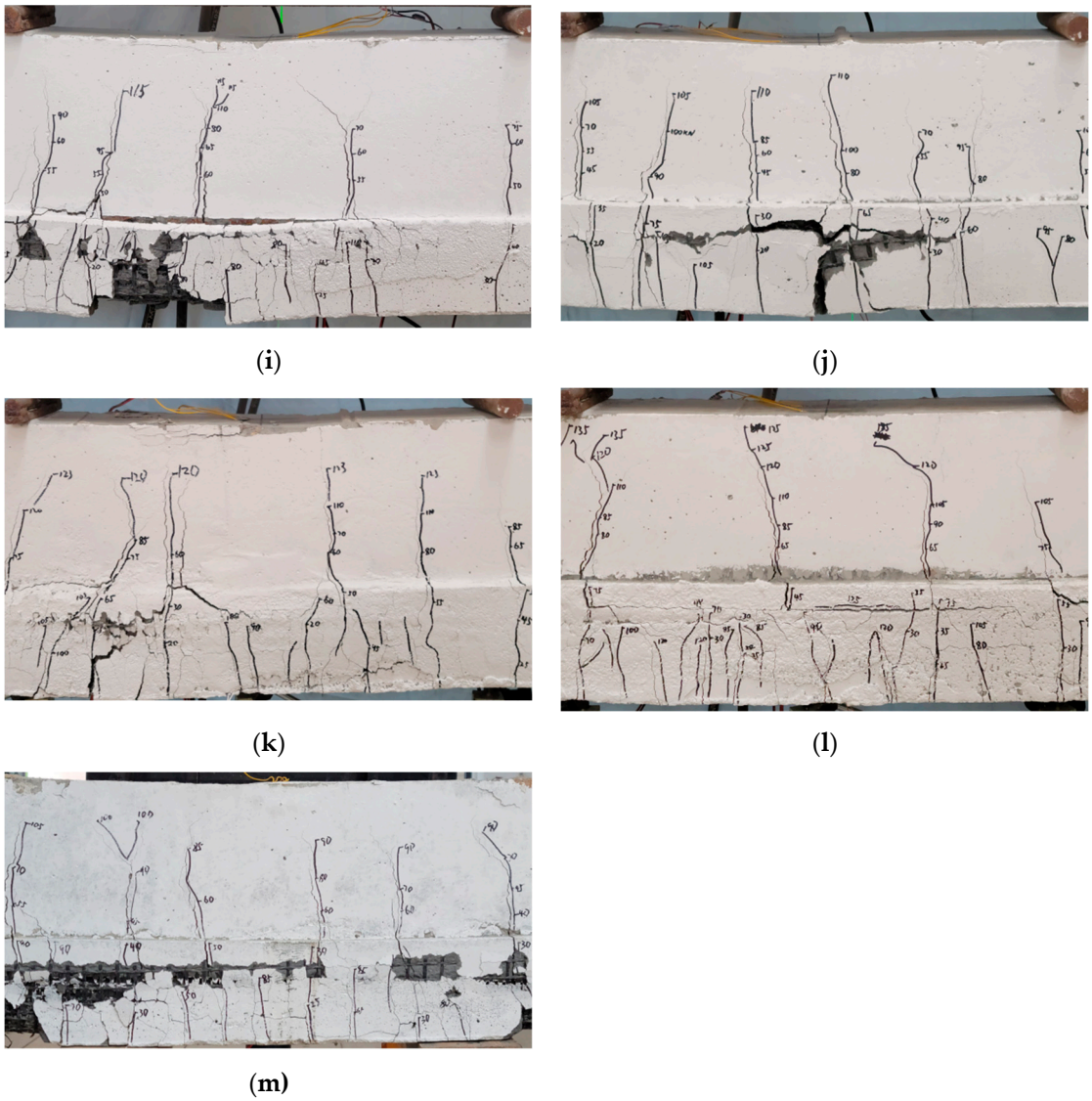

Figure 7. Failure modes of specimens: (**a**) M-0; (**b**) M-5; (**c**) M-10; (**d**) M-15; (**e**) M-5-SL2A; (**f**) M-5-TL2A; (**g**) M-5-TL2B; (**h**) M-10-SL2A; (**i**) M-10-TL2A; (**j**) M-10-TL1B; (**k**) M-10-TL2B; (**l**) M-10-TL3B; (**m**) M-15-TL2B.

These four failure modes of FRCM-strengthened corroded RC beam also reported in the research of [23].

3.2. Crack Analysis

Figure 7a–d shows the crack patterns in the reference beam M-0 and corrosion-only beams M-5, M-10, and M-15. As mentioned previously, these four beams were not strengthened with TRC. A comparison between the figures shows that the numbers of cracks in the pure bending section of the corrosion-only RC beams M-0, M-5, M-10, and M-15 are seven, three, three, and two, respectively. This phenomenon indicates that the more serious the degree of corrosion of the tensile steel bar, the fewer the number of cracks in the RC beam. This is because the bonding performance between the tensile steel bars and concrete was degeneration due to the corrosion of the tensile steel bars. Figure 7g,k,m shows that the M-5-TL2B, M-10-TL2B, and M-15-TL2B beams have the same number of cracks, which is six. These beams had a significantly greater number of cracks than the corrosion-only RC

beam, and only one less than that in the reference RC beam M-0. This shows that the TRC plays a role in increasing the number of cracks in corroded RC beams.

Figure 8a shows the maximum crack widths of the reference RC beam M-0 and corrosion-only RC beams M-5, M-10, and M-15 under different loads. As shown, the crack widths of the reference RC beam M-0 and corrosion-only RC beams M-5, M-10, and M-15 increases under the same load level, indicating that the corrosion of the steel bars led to the widening of the crack in the RC beams. This phenomenon is also due to the decrease in the bonding performance between the steel bars and concrete. Figure 8a also shows that the cracks in the TRC-strengthened corroded beam (M-5-TL2R, M-10-TL2R, and M-15-TL2R) have an evidently smaller width than those in the corrosion-only RC beams (M-5, M-10, and M-15) at the same corrosion rate and under the same load. This demonstrates that the width of the cracks in corroded RC beams can be reduced using TRC.

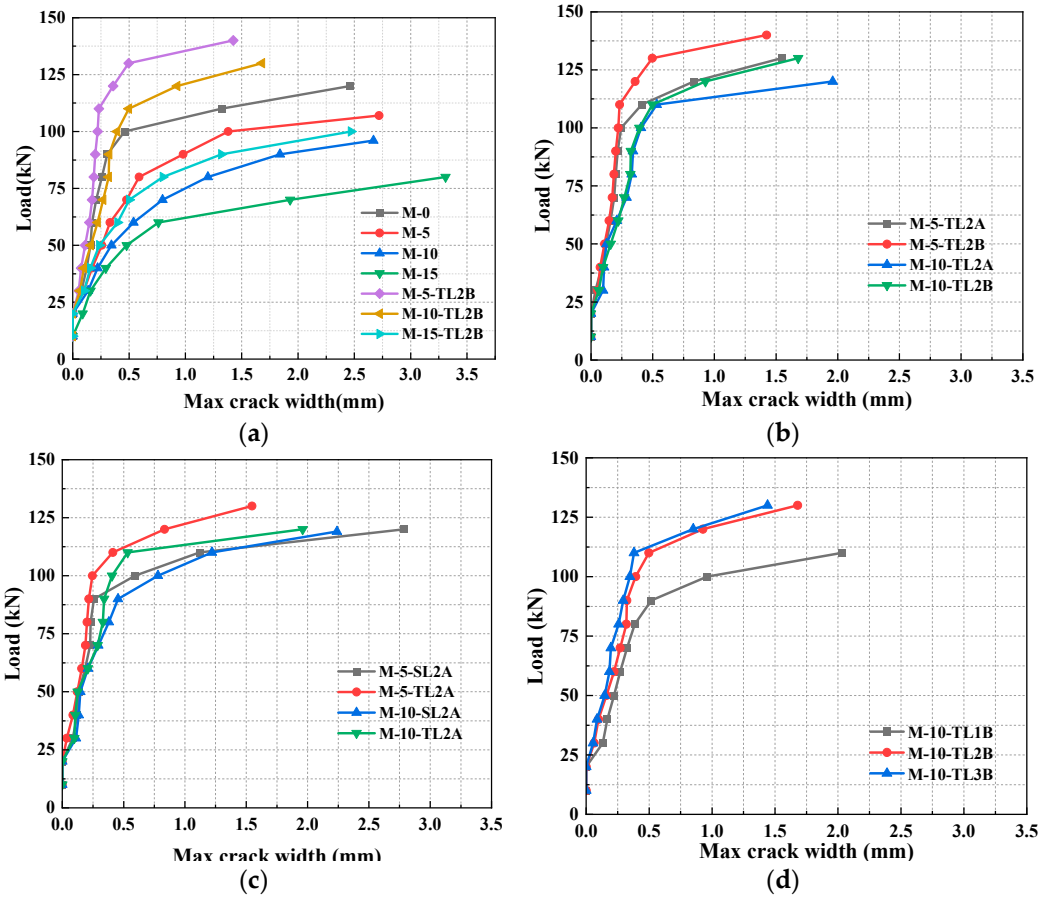

Figure 8. Load versus maximum crack width of each specimen: (**a**) non-strengthened vs. strengthened; (**b**) different strengthening methods; (**c**) different strengthening schemes; (**d**) different number of textile layers added.

3.2.1. Effect of Strengthening Method

Figure 7f,g shows the crack patterns in M-5-TL2A and M-5-TL2B, respectively. Clearly, the number of cracks in the pure bending sections of M-5-TL2A and M-5-TL2B in the concrete part were 4 and 6, respectively. This shows that strengthening method B was better in terms of controlling the number of cracks. This is attributed to the improvement in the properties of the bonding between the corroded steel bar and concrete after repairing. A comparison between M-10-TL2A (Figure 7i) and M-10-TL2B (Figure 7k) shows the same phenomenon.

Figure 8b shows the maximum widths of the cracks in the M-5-TL2A, M-5-TL2B, M-10-TL2A, and M-10-TL2B beams under different loads. The M-5-TL2B beam had a slightly greater maximum crack width than the M-5-TL2A beam before the yielding of the steel bar.

The maximum crack width of the M-5-TL2B beam was greater than that of the M-5-TL2A beam after the yielding of the steel bar; this is again attributed to the improvement in the bonding properties between the corroded steel bar and concrete brought about by repairing.

3.2.2. Effect of Strengthening Scheme

From Figure 7h,i, the numbers of cracks in the concrete part of the M-10-SL2A and M-10-TL2A beams are 3 and 5, respectively. From Figure 7e,f, the numbers of cracks in the concrete part of the M-5-SL2A and M-5-TL2A beams are 3 and 4, respectively. This result shows that the three-sided strengthening scheme outperformed the single-sided scheme in terms of controlling the number of cracks.

Figure 8c shows the maximum crack width under the different strengthening schemes. The maximum width of the cracks in the M-5-SL2A beam was slightly greater than that of the cracks in the M-5-TL2A beam before the yielding of the steel bar. The maximum crack width of M-5-SL2A was greater than that of M-5-TL2A after the yielding of the steel bar. This once again demonstrates that the three-sided scheme slightly outperformed the single-sided strengthening scheme.

3.2.3. Effect of the Number of Textile Layers Added

Figure 7j shows the crack pattern in the M-10-TL1B beam. It has seven cracks in the concrete part, which is equal to the number of cracks in M-0 and greater than that in M-10. This phenomenon demonstrates that the TRC could increase the number of cracks and reduce the crack space in terms of strengthening the corroded RC beams. Figure 7k,l show that the numbers of cracks in the concrete part of the M-10-TL2B and M-10-TL3B beams are 6 and 4, respectively. M-10-TL3B had fewer cracks than M-10-TL1B and M-10-TL2B. This may be attributed to the different failure modes.

Figure 8d shows the maximum width of the cracks in M-10-TL1B, M-10-TL2B, and M-10-TL3B under different load levels. As shown, the crack width decreased under the same load level. This indicates that the width of the cracks in TRC-strengthened corroded RC beams decreases with the increase in the number of textile layers added.

3.3. Bearing Capacity Analysis

Table 4 lists the P_y (yield load) and P_u (ultimate load) values of each test beam. Compared with the reference RC beam M-0, the yield loads of the corrosion-only beams M-5, M-10, and M-15 were reduced by 12.54%, 20.51%, and 41.03%, respectively, and their ultimate bearing capacities were reduced by 10.33%, 18.82%, and 33.55%, respectively. Therefore, it can be concluded that the standardcorrosion of the tensile steel bars significantly influenced the bearing capacity of the RC beams, and with the increase in the corrosion rate, the yield and ultimate loads of the beams decreased further.

Compared with the corrosion-only beam M-5, the P_y and P_u values of M-5-TL2B increased by 41.04% and 28.57%, respectively. Compared with the corrosion-only beam M-10, P_y and P_u of M-10-TL2B increased by 34.05% and 29.49%, respectively. Compared with the corrosion-only beam M-15, P_y and P_u of M-15-TL2B increased by 42.51% and 33.73%, respectively. Moreover, the P_y and P_u values of M-5-TL2R and M-10-TL2R were greater than those of the reference beam M-0. These results indicate that the TRC could effectively improve the P_y and Pu values of the corroded RC beams. The yield load of the corroded beams increased because the tensile stress in the corroded steel bar could be shared by the textile. The increase in the ultimate load could be attributed to the reinforcement effect of the TRC.

The study of Ref. [23] also showed that FRCM can improve the yield load and ultimate load of corroded RC beams. However, the increase range is different from this study. The reason is that the mechanical property of the textile and matrix used in Ref. [23] is different from this study.

Table 4. Summary of test results.

Spec.	η_1/%	η_2/%	P_y/kN	Δ_y/mm	P_u/kN	δ_u/mm	$(P_y-P_{y,M-0})/P_{y,M-0}$	$(P_u-P_{u,M-0})/P_{u,M-0}$	EAI
M-0	-	-	105.3	10.34	124.9	44.76	-	-	3040
M-5	5	4.78	92.1	9.47	112	31.55	−12.54%	−10.33%	2365
M-10	10	9.95	83.7	9.36	101.4	29.4	−20.51%	−18.82%	2173
M-15	15	17.14	62.1	6.67	83	17.37	−41.03%	−33.55%	1095
M-5-SL2A	5	4.24	113	8.10	127	33.55	7.31%	1.68%	2713
M-5-TL2A	5	5.47	123.6	8.47	139.6	36.00	17.38%	11.77%	3290
M-5-TL2B	5	5.13	129.9	8.33	144	29.42	23.36%	15.29%	3094
M-10-SL2A	10	8.76	103.4	10.58	119.1	37.87	−1.80%	−4.64%	2027
M-10-TL2A	10	11.05	108.3	8.34	122	33.54	2.85%	−2.32%	2494
M-10-TL2B	10	12.79	112.2	10.27	131.3	39.44	6.55%	5.12%	2475
M-10-TL1B	10	11.01	97.1	8.79	111.5	32.02	−7.79%	−10.73%	1997
M-10-TL3B	10	12.42	118.3	9.45	137.6	40.91	12.35%	10.17%	3445
M-15-TL2B	15	16.05	88.5	12.16	111	41.83	−15.95%	−11.13%	2361

Note: η_1 is theoretical corrosion rate; η_2 is actual corrosion rate; P_y is the yielding load; δ_y is the mid-span deflection at the yielding load; P_u is the ultimate load; δ_u is the mid-span deflection at the ultimate load; EAI is the energy absorption index.

3.3.1. Effect of the Strengthening Scheme

As shown in Table 4, the P_y and Pu values of M-5-SL2A are 113 kN and 127 kN, and those of M-5-TL2A, are 123.6 kN and 139.6 kN, respectively. This demonstrates that the improvement in the bearing capacity brought about by the three-sided scheme was better than that brought about by the single-sided scheme. This is because in the three-sided scheme, the TRC was also applied to the other two sides of the beam, which is equivalent to increasing the reinforcement ratio.

As listed in Table 4, the P_y and P_u values of M-5-SL2A increased by 7.31% and 1.68% compared with that of M-0. The Py and Pu values of M-5-TL2A increased by 17.38% and 11.77% compared with that of M-0, respectively. These results demonstrate that both the single-sided and three-sided schemes were effective and could improve the bearing capacity of the corroded RC beams.

3.3.2. Effect of the Strengthening Method

As shown in Table 4, the P_y and P_u values of M-5-TL2A are 123.6 kN and 139.6 kN, and those of M-5-TL2B, are 129.9 kN and 144.0 kN, respectively. This demonstrates that the improvement in the bearing capacity brought by strengthening method B was better than that brought by strengthening method A, owing to the better bonding performance between the concrete and steel bar. A comparison between M-10-TL2A and M-10-TL2B showed the same law.

3.3.3. Effect of the Number of Textile Layer Added

M-10-TL1B, M-10-TL2B, and M-10-TL3B beams exhibited yield loads of 97.1, 112.2, and 118.3 kN, respectively. M-10-TL1R had a lower yield load than M-0 (105.3 kN). The yield loads of the two other beams were greater than that of M-0. The ultimate loads of M-10-TL1B, M-10-TL2B, and M-10-TL3B were 111.5, 131.3, and 137.6 kN, respectively. The ultimate load of M-10-TL1R was lower than that of M-0 (124.9 kN). The ultimate loads of the two other beams were greater than that of M-0. This shows that increasing the number of textile layers could effectively improve the bearing capacity of the corroded RC beams, and their yield and ultimate loads increased with the increase in the number of textile layers added.

3.4. Load–Displacement Response

Figure 9 shows the load–displacement curves of each test beam. Clearly, most of the test beams have similar load–displacement curves, exhibiting a three-stage characteristic.

The first stage is the pre-cracking stage, and the stiffness in this stage is the highest. The second stage is from cracking to steel yielding, and the stiffness in this stage decreases. The third stage is from yielding to failure, and the stiffness here is further reduced. The turning points related to the cracking and yielding can be reflected on the load–displacement curve.

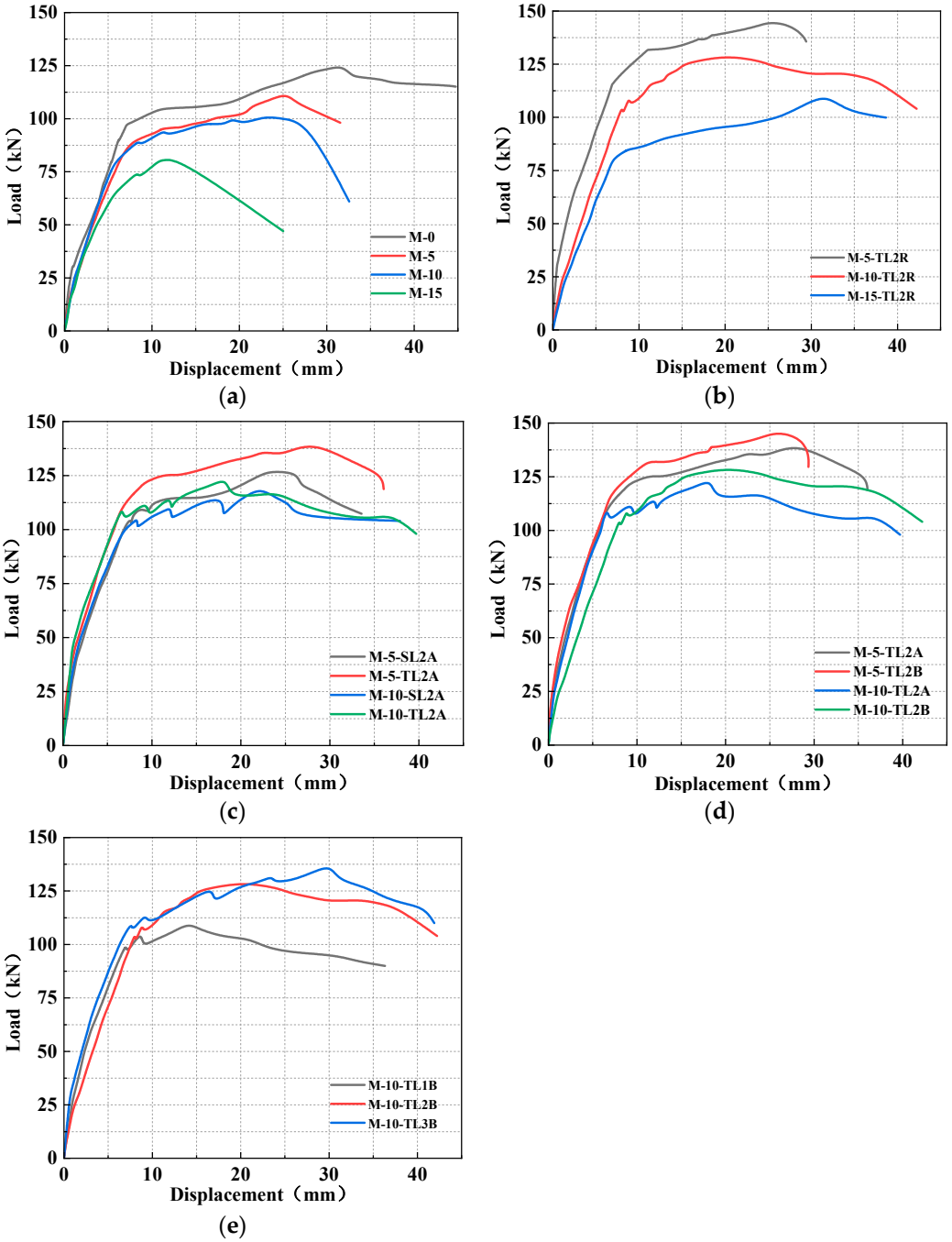

Figure 9. Load–displacement curves of each specimen: (**a**) non-strengthened beams; (**b**) strengthened beams with different corrosion rates; (**c**) different strengthening schemes; (**d**) different strengthening methods; (**e**) different number of textile layers added.

Figure 9a shows the load–displacement curves of the reference beam M-0 and corrosion-only beams M-5, M-10, and M-15. Clearly, the corroded beam does not show an evident cracking stage. The pre-yield stiffness of the corrosion-only beams was lower than that of the reference beams, and the greater the corrosion rate, the lower the pre-yield stiffness of the beams. When the corrosion rate reached 15%, the load–displacement curve of the

corroded beam changed significantly, the yield point becomes not evident, and the third stage almost disappeared, indicating certain brittle characteristics. This may be because of the deterioration in the mechanical properties of the steel bars after corrosion to a certain extent. In ref. [30], when the corrosion rate of steel bars exceeds a certain value, the stress–strain curve changed, the yield platform disappeared, the ductility deteriorated, the softening stage disappeared, and there was brittle fracture. A comparison between Figure 9a,b shows that the load–displacement curve of M-15-TL2B is different from that of M-15. The load–displacement curve of M-15-TL2B shows the three-stage characteristic, indicating that the failure mode has ductile characteristics. The load–displacement curve of M-15 does not exhibit the three-stage failure characteristic, and the failure mode has brittle characteristics. Thus, it can be concluded that the TRC can not only improve the bearing capacity of corroded beams, but also change the failure mode.

Figure 9c shows the load–displacement curves of M-5-SL2A, M-5-TL2A, M-10-SL2A, and M-10-TL2A. The load–displacement curves of these four beams have the three-stage characteristics. Moreover, the stiffness of M-5-TL2A in the second stage was higher than that of M-5-SL2A. A comparison between M-10-TL2A and M-10-SL2A showed the same phenomenon. This demonstrated that the stiffness improvement in the second stage brought about by the three-sided scheme was better than that brought about by the single-sided scheme. Figure 9d shows that the stiffnesses in the second stage of M-5-TL2A, M-5-TL2B, and M-10-TL2A are very similar, and this stiffness value is slightly greater than that of M-10-TL2B. Considering the discreteness of the test results, the strengthening method had little effect on the stiffness. Figure 9e shows the load–displacement curves of M-10-TL1B, M-10-TL2B, and M-10-TL3B. Clearly, the third stage in the M-10-TL3B beam was shorter than that in the other two beams. This is because M-10-TL3B exhibited a debonding failure mode. Moreover, the stiffnesses in the second stage of M-10-TL1B, M-10-TL2B, and M-10-TL3B are relatively close. This shows that increasing the number of textile layers had little effect on the stiffness of the beam in the second stage.

3.5. Ductility Performance

In this study, the ductility of the test beam can be evaluated in terms of the energy absorption index (EAI), which is defined as the area of the load–displacement curve from the beginning of loading to the maximum load. The better the ductility of the test beam, the greater EAI.

Figure 10 shows the histogram of the EAI of each specimen. As shown, the EAI values of the corrosion-only beams (M-5, M-10, and M-15) are 2365, 2173, and 1095, respectively. The EAI values of M-5-TL2B, M-10-TL2B, and M-15-TL2B are 3094, 2475, and 2361, respectively. This phenomenon demonstrates that the corrosion significantly influences the ductility of both the common RC beam and the TRC-strengthened beam, and with the increase in the corrosion rate, the ductility of both beams decreases. This is because, on the one hand, the corrosion weakens the bonding performance between the steel and concrete, and on the other hand, it deteriorates the ductility of the steel bars [30]. The EAI values of M-5-TL2B, M-10-TL2B, and M-15-TL2B were 1.31, 1.14, and 2.16 times higher than those of the corrosion-only beams M-5, M-10, and M-15, respectively. Moreover, the ductility index of some of the TRC-strengthened beams (M-5-TL2A, M-5-TL2B, and M-10-TL3B) had exceeded that of M-0. This phenomenon illustrates that the use of TRC is known to have a significant effect on improving the ductility of corroded RC beams.

As shown in Figure 10, the EAI values of M-5-SL2A and M-5-TL2A are 2713 and 3290, respectively. The EAI values of M-10-SL2A and M-10-TL2A are 2027 and 2494, respectively. This showed that the three-sided strengthening scheme is superior to the single-sided strengthening scheme in terms of improving the ductility. This is mainly because the number of textile layers in the three-sided strengthening scheme was greater than that in the single-sided strengthening scheme. The EAI values of M-5-TL2A and M-5-TL2B were 3290 and 3094, respectively. The EAI values of M-10-TL2A and M-10-TL2B were 2494 and 2475, respectively. This shows that whether the concrete cover is removed before

strengthening had little effect on the ductility. Figure 10 also clearly shows that the EAI values of M-10-TL1B, M-10-TL2B, and M-10-TL3B are 1997, 2475, and 3445, respectively, indicating an improvement in the ductility of TRC-strengthened corroded beams with increasing the number of textile layers. This is because, with the increase in the number of textile layers, the yield and ultimate loads were improved. Therefore, the area under the load–displacement curve increased, and the EAI also increased.

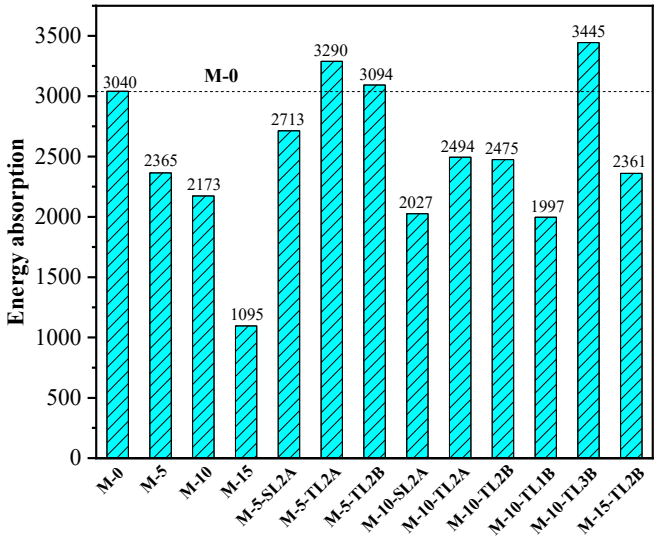

Figure 10. Energy absorption diagrams.

4. Conclusions

The experimental results presented in this paper proved the potential of TRC to be used in strengthening corrosion-damage RC beams to improve their flexural behavior, and can help advance the strengthening design of corroded beams, particularly those employed in a marine environment, where steel bars undergo frequent corrosion. The main results are as follows:

(1) Four different failure modes of the TRC-strengthened corroded RC beams were observed in this test, including flexural failure, partial debonding of the TRC, textile separation from the matrix, and fiber slip accompanied by matrix shedding.
(2) The three-sided strengthening scheme outperformed the single-sided scheme in controlling the number of cracks. Increasing the number of textile layers can reduce the crack width of the strengthened beams.
(3) In terms of improving bearing capacity of the corroded RC beam, the three-sided scheme was better than that of the single-sided scheme, and strengthening method B outperformed strengthening method A.
(4) The EAI of the TRC-strengthened corroded beam increased with the increase in the number of textile layers. When a beam with a corrosion rate of 10% was strengthened with a three-layer textile, the EAI of this beam exceeded that of the reference RC beam.
(5) Further investigations should be focused on the shear behavior of corroded RC beams strengthened with TRC, aiming at providing design methodologies and recommendations.

Author Contributions: Conceptualization, W.X. and J.S.; Data curation, Z.Y. and G.D.; Supervision, Y.L.; Investigation, Y.L.; Methodology, Y.L.; Writing—original draft preparation, W.X. and Z.Y.; Writing—review and editing, J.S. and G.D. All authors have read and agreed to the published version of the manuscript.

Funding: This research was funded by the National Natural Science Foundation of China, grant number 52008387, the China Postdoctoral Science Foundation funded project, grant number 2019M652008, and Henan Province Science and Technology Project, grant number 232102241010.

Data Availability Statement: The data presented in this study are available on request from the corresponding author. The data are not publicly available due to the contract between us and the work unit.

Conflicts of Interest: The authors declare no conflict of interest.

References

1. Azad, A.K.; Ahmad, S.; Azher, S.A. Residual strength of corrosion-damaged reinforced concrete beams. *ACI Mater. J.* **2007**, *104*, 40–47.
2. Stewart, M.G.; Al-Harthy, A. Pitting corrosion and structural reliability of corroding RC structures: Experimental data and probabilistic analysis. *Reliab. Eng. Saf.* **2008**, *93*, 373–382. [CrossRef]
3. Zhang, R.; Castel, A.; François, R. Concrete cover cracking with reinforcement corrosion of RC beam during chloride-induced corrosion process. *Cem. Concr. Res.* **2010**, *40*, 415–425. [CrossRef]
4. Duprat, F. Reliability of RC beams under chloride-ingress. *Constr. Build. Mater.* **2007**, *21*, 1605–1616.
5. Val, D.V.; Trapper, P.A. Probabilistic evaluation of initiation time of chloride-induced corrosion. *Reliab. Eng. Saf.* **2008**, *93*, 364–372. [CrossRef]
6. Masoud, S.; Soudki, K. Evaluation of corrosion activity in FRP repaired RC beams. *Cem. Concr. Comp.* **2006**, *28*, 969–977. [CrossRef]
7. Malumbela, G.; Moyo, P.; Alexander, M. Load-bearing capacity of corroded, patched and FRP-repaired RC beams. *Mag. Concr. Res.* **2011**, *63*, 797–812. [CrossRef]
8. Zheng, A.; Liu, Z.; Li, F.; Li, S. Experimental investigation of corrosion-damaged RC beams strengthened in flexure with FRP grid-reinforced ECC matrix composites. *Eng. Struct.* **2021**, *244*, 112779. [CrossRef]
9. Peled, A. Confinement of danaged and nondamaged structural concrete with FRP and TRC Seeves. *ASCE J. Compos. Constr.* **2007**, *11*, 514–522. [CrossRef]
10. Dai, J.G.; Yokota, H.; Iwanami, M.; Kato, E. Experimental investigation of the influence of moisture on the bond behavior of FRP to concrete interfaces. *ASCE J. Compos. Constr.* **2010**, *14*, 834–844. [CrossRef]
11. Larbi, A.S.; Agbossou, A.; Hamelin, P. Experimental and numerical investigations about textile-reinforced concrete and hybrid solutions for repairing and/or strengthening reinforced concrete beams. *Compos. Struct.* **2013**, *99*, 152–162. [CrossRef]
12. Yin, S.P.; Sheng, J.; Wang, X.X.; Li, S.G. Experimental investigations of the bending fatigue performance of TRC-strengthened RC beams in conventional and aggressive chlorate environments. *ASCE J. Compos. Constr.* **2016**, *20*, 04015051. [CrossRef]
13. D'Ambrisi, A.; Focacci, F. Flexural strengthening of RC beams with cement-based composites. *ASCE J. Compos. Constr.* **2011**, *15*, 707–720. [CrossRef]
14. Ombres, L. Flexural analysis of reinforced concrete beams strengthened with a cement based high strength composite material. *Compos. Struct.* **2011**, *94*, 143–155. [CrossRef]
15. Yin, S.; Na, M.; Yu, Y.; Wu, J. Research on the flexural performance of RC beams strengthened with TRC under the coupling action of load and marine environment. *Constr. Build. Mater.* **2017**, *132*, 251–261. [CrossRef]
16. Sheng, J.; Wang, L.-C.; Yin, S.-P. Study on the mechanical performance of TRC-strengthened RC beams under a salt freeze-thaw environment. *Cold Reg. Sci. Technol.* **2021**, *192*, 103384. [CrossRef]
17. Mazzuca, P.; Ombres, L.; Guglielmi, M.; Verre, S. Residual Mechanical Properties of PBO FRCM Composites after Elevated Temperature Exposure: Experimental and Comparative Analysis. *J. Mater. Civ. Eng. ASCE* **2023**, *35*, 04023383. [CrossRef]
18. Ombres, L.; Mazzuca, P. Residual Flexural Behavior of PBO FRCM-Strengthened Reinforced Concrete Beams after Exposure to Elevated Temperatures. *J. Compos. Constr. ASCE* **2023**, *28*, 04023063. [CrossRef]
19. Elsanadedy, H.M.; Almusallam, T.H.; Alsayed, S.H.; Al-Salloum, Y.A. Flexural strengthening of RC beams using textile reinforced mortar-experimental and numerical study. *Compos. Struct.* **2013**, *97*, 40–55. [CrossRef]
20. El-Maaddawy, T.; El Refai, A. Innovative repair of severely corroded T-beams using fabric-reinforced cementitious matrix. *ASCE J. Compos. Constr.* **2016**, *20*, 04015073. [CrossRef]
21. Elghazy, M.; El Refai, A.; Ebead, U.; Nanni, A. Effect of corrosion damage on the flexural performance of RC beams strengthened with FRCM composites. *Compos. Struct.* **2017**, *180*, 994–1006. [CrossRef]
22. Elghazy, M.; El Refai, A.; Ebead, U.; Nanni, A. Post-repair flexural performance of corrosion-damaged beams rehabilitated with fabric-reinforced cementitious matrix (FRCM). *Constr. Build. Mater.* **2018**, *166*, 732–744. [CrossRef]
23. Elghazy, M.; El Refai, A.; Ebead, U.; Nanni, A. Fatigue and monotonic behaviors of corrosion-damaged reinforced concrete beams strengthened with FRCM composites. *ASCE J. Compos. Constr.* **2018**, *22*, 04018040. [CrossRef]
24. Feng, R.; Liu, Y.; Zhu, J.H.; Xing, F. Flexural behaviour of C-FRCM strengthened corroded RC continuous beams. *Compos. Struct.* **2020**, *245*, 112200. [CrossRef]
25. *Chinese Standard GB/T 50010-2010*; Code for Design of Concrete Structures. Chinese Building Press: Beijing, China, 2010.
26. *Chinese Standard GB/T 50107-2010*; Standard for Evaluation of Concrete Compressive Strength. Chinese Building Press: Beijing, China, 2010.
27. *Chinese Standard GB/T 228.1-2010*; Metallic Materials Tensile Test Part 1: Method of Test at Room Temperature. Chinese Building Press: Beijing, China, 2010.

28. *Chinese Standard GB/T 1447-2005*; Fiber-Reinforced Plastics Composites—Determination of Tensile Properties. Chinese Building Press: Beijing, China, 2005.
29. *Chinese Standard JGJ/T70-2009*; Standard for Test Method of Performance on Building Mortar. Chinese Building Press: Beijing, China, 2010.
30. Sheng, J.; Xia, J. Effect of simulated pitting corrosion on the tensile properties of steel. Constr. *Build. Mater.* **2017**, *131*, 90–100. [CrossRef]

Disclaimer/Publisher's Note: The statements, opinions and data contained in all publications are solely those of the individual author(s) and contributor(s) and not of MDPI and/or the editor(s). MDPI and/or the editor(s) disclaim responsibility for any injury to people or property resulting from any ideas, methods, instructions or products referred to in the content.